ISSN 1070-4272, Russian Journal of Applied Chemistry, 2017, Vol. 90, No. 1, pp. 138−143. © Pleiades Publishing, Ltd., 2017.

VARIOUS TECHNOLOGICAL PROCESSES

Synthesis of CuO Nanoparticles via One-pot Wet-chemical Method and Its Catalytic Performance on the Thermal Decomposition of Ammonium Perchlorate[1]

Bowen Xue, Zhongwen Qian, Chunsheng Liu, and Genxiang Luo*

School of Chemistry and Materials Science, Liaoning Shihua University, Fushun 113001, People's Republic of China
**e-mail: gxluo1965@163.com*

Received December 21, 2016

Abstract—Sphere-like CuO products aggregated by numerous nanoparticles were fabricated by a low-temperature (50°C) wet chemical method using $CuSO_4 \cdot 5H_2O$ as precursor. The possible formation processes of CuO were investigated by a series of single-factor experiments. The CuO was characterized by X-ray diffraction, scanning electron microscopy, transmission electron microscopy, high-resolution transmission electron microscopy, selected-area electron diffraction. Furthermore, the application of CuO nanoparticles on the thermal decomposition of ammonium perchlorate was studied with 2 wt % CuO nanoparticles at heating rates of 10, 15, 20, and 25°C min^{-1} from 35 to 500°C.

DOI: 10.1134/S1070427217010207

INTRODUCTION

CuO, a p-type semiconductor with a narrow band gap of 1.2 eV, has attracted a great attention for its applications in catalysis [1, 2], Li-ion electrode material [3], solar cells [4], sensors [5, 6], solar selective absorbing coating [7], etc.

The size and shape of CuO nanostructures control the properties of CuO, which determine the activity of CuO [8]. The methods of CuO fabrication include precipitation method [9], ultrasonic irradiation [10], thermal treatment [11], hydrothermal method [12, 13], ionothermal route [14], ball-milling method [15], electrochemical route [16], wet chemical route [17, 18], etc. Among the various routes, wet chemical route was one of the most promising synthesis methods because of its low cost, high yield and high-quality production [17]. Whereas, the normal routes of the synthesis process of CuO are tedious.

Recently, Ba et al. [19], Shaabani et al. [20], and Zhu et al. [21] prepared CuO nanostructures via an intermediate of $Cu(OH)_2$ by combining wet chemical method with thermal decomposition method. Darezereshki et al. [22], Zhang et al. [23], Bakhtiari et al. [24] and Zhang et al. [25] synthesized CuO nanostructures from basic copper salts by direct thermal decomposition method.

The one-pot wet-chemical method is simple and environmentally friendly in the fabrication of CuO due to its low temperature, mild alkaline conditions, and short reaction time. In our initial work [26], CuO was prepared from $Cu_2CO_3(OH)_2$ by wet chemical method. In this article, an one-pot synthesis of CuO nanoparticles from copper salt in alkaline condition through wet chemical route was fabricated. The possible pathways of CuO nanoparticles were studied through a series of control experiments. Also, CuO nanoparticles were applied to the thermal decomposition of ammonium perchlorate (AP).

EXPERIMENTAL

Materials. The reagents including $CuSO_4 \cdot 5H_2O$, Na_2CO_3, NH_4ClO_4, anhydrous ethanol were all of analytical grade and used in this work without any further purification. Distilled water was used throughout the experiments.

Synthesis of CuO nanoparticles. In a typical process, Na_2CO_3 (0.003 mol 0.3180 g) was dissolved in 50 mL

[1] The text was submitted by the authors in English.

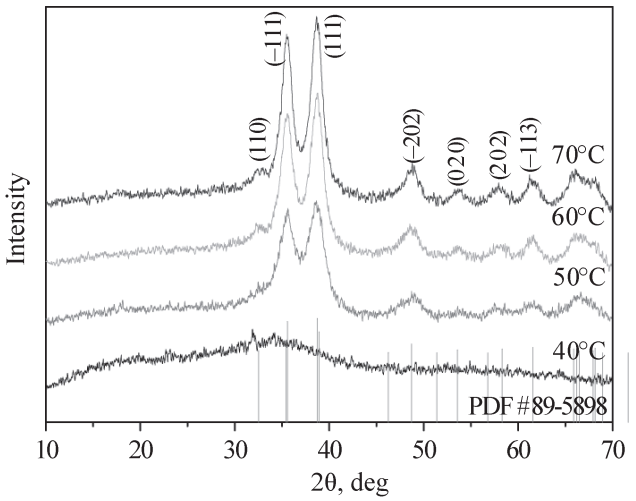

Fig. 1. XRD pattern of CuO samples with different reaction temperatures.

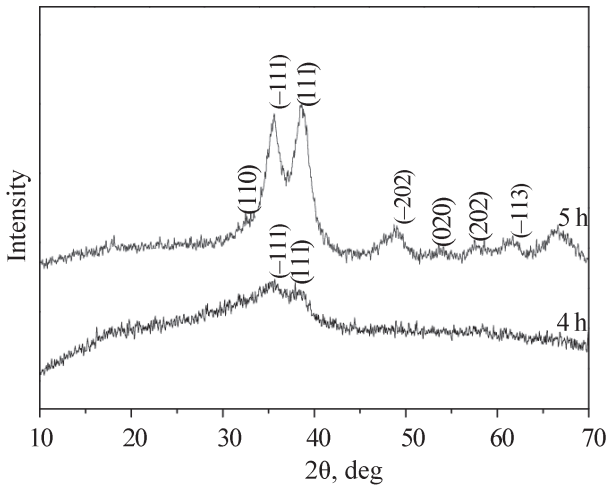

Fig. 2. XRD pattern of CuO samples with different reaction time.

distilled water to form 0.06 mol L^{-1} Na_2CO_3 aqueous solution. 0.001 mol 0.2497 g $CuSO_4 \cdot 5H_2O$ was added in the above solution with constant stirring. The reaction mixture was kept in water bath at 70°C for 5 h. The precipitate was centrifuged and washed with distilled water and anhydrous ethanol for several times. The final products were dried at 60°C and collected for characterization.

Characterization. X-ray diffraction (XRD, D/max–RB 12 kW) with CuK_α radiation of 0.15418 nm was used to characterize the structure of prepared samples with 2θ ranging from 10° to 70°. The average crystal size of products was calculated by Debye–Scherrer equation [9],

$$D = \frac{k\lambda}{\beta\cos\theta}, \quad (1)$$

where D is the main size of the crystalline domains, k is the Scherrer constant (0.89), λ is the X-ray wavelength (0.15418), β is the line broadening at half maximum of the diffraction peak, and θ is the diffraction angle.

The morphology of the products was investigated by a SU800 scanning electron microscope (SEM, Hitachi, Japan). Transmission electron microscopy (TEM), high-resolution transmission electron microscopy (HRTEM), and selected–area electron diffraction (SAED) were performed on a JEOL 2200FS transmission electron microscopy at an accelerating voltage of 200 kV. The sample for TEM analysis was firstly managed by ultrasonic dispersion in 10 mL ethanol for 1 min. The products above were dropped on a carbon-coated copper grid and dried in room temperature.

Catalytic thermal decomposition of AP. Simultaneous differential scanning calorimetry and thermogravimetric analysis (DSC–TGA, TA Instruments SDT 2960) technique was used to evaluate the catalytic activity of CuO nanoparticles in the thermal decomposition of AP, with a CuO/AP mess ration of about 2 : 98.

CuO and AP were completely mixed by grinding method. The test was applied with a heating rate of 10°C min^{-1} in a temperature range of 35–500°C with the N_2 flow rate of 50 mL min^{-1}.

RESULT AND DISCUSSION

The optimal condition of CuO synthesis was studied by single-factor experiments. XRD patterns of the products synthesized through various conditions are displayed in Figs. 1–3. Figure 1 represents the synthesis of CuO with different temperatures. $CuSO_4 \cdot 5H_2O$ (0.2497 g) and 50 mL 0.06 M Na_2CO_3 aqueous solution were heated at different temperatures (40, 50, 60, and 70°C, respectively) for 5 h. When the temperature exceeds 50°C , all the peaks of diffraction are in agreement with the standard date from JCPDS card no. 89-5898. No impurity peaks exist among all the diffraction peaks. It indicates that the starting materials were converted into CuO completely. However, when the temperature is 40°C, none of the diffraction peaks match with the standard CuO XRD pattern.

In Figure 2, 0.2497 g $CuSO_4 \cdot 5H_2O$ and 50 mL 0.06 M Na_2CO_3 aqueous solution were heated at 50°C for 4 and 5 h, respectively. When the reaction time is 4 h, two

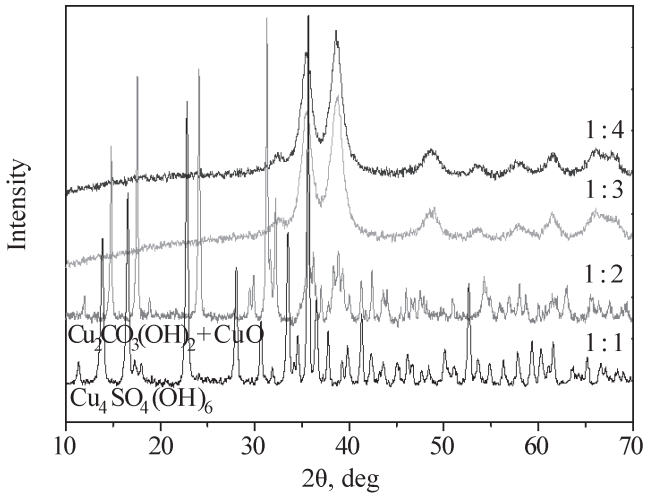

Fig. 3. XRD pattern of CuO samples with different molar ratios of $CuSO_4 \cdot 5H_2O$ to Na_2CO_3.

peaks of diffraction were matched with the standard CuO XRD pattern. The products are CuO with a low degree of crystalline. Whereas, when the reaction time exceeds 5 h, all of the peaks are consistent with CuO XRD pattern.

Figure 3 shows the reaction of $CuSO_4 \cdot 5H_2O$ and Na_2CO_3 with different molar ratio at 50°C for 5 h. $Cu_4SO_4(OH)_6$ was synthesized with a molar ratio about 1 : 1, without any impurities. CuO was synthesized when the molar ratio of $CuSO_4 \cdot 5H_2O$ to Na_2CO_3 was 1 : 2, but $Cu_2CO_3(OH)_2$ exists as a impurity. When the reaction molar ratios of $CuSO_4 \cdot 5H_2O$ to Na_2CO_3 are 1 : 1 and 1 : 2, the intermediates are $Cu_4SO_4(OH)_6$ and $Cu_2CO_3(OH)_2$, respectively. The results above are in agreement with the report of Parekh et al. [27]. When the $CuSO_4 \cdot 5H_2O$: Na_2CO_3 molar ratio is over 2, $Cu_2CO_3(OH)_2$ continues reacting with OH^-. Therefore, $Cu_2CO_3(OH)_2$ was as an intermediate in the process of CuO synthesis. When the molar ratio of $CuSO_4 \cdot 5H_2O$ and Na_2CO_3 was 1 : 3 and 1 : 4, the diffraction peaks corresponded to the standard CuO XRD pattern without any impurities.

The solubility products of $Cu_4SO_4(OH)_6$ and $Cu_2CO_3(OH)_2$ are $\log K_{sp(Cu_4SO_4(OH)_6)} = -17.3$ and $\log K_{sp(Cu_2CO_3(OH)_2)} = -31.96$ [28], respectively. According to the XRD analysis above, the possible pathways of CuO synthesis were deduced as shown in Eqs. (2)–(6).

$$CO_3^{2-} + H_2O \rightarrow CO_2 + 2OH^-, \quad (2)$$

$$CO_2 + H_2O + CO_3^{2-} \rightarrow 2HCO_3^-, \quad (3)$$

$$2Cu^{2+} + SO_4^{2-} + 6OH^- \rightarrow Cu_4SO_4(OH)_6^-, \quad (4)$$

$$Cu_4SO_4(OH)_6^- + 2CO_3^{2-} + 2H^+ \rightarrow 2Cu_2CO_3(OH)_2 + SO_4^{2-} + 2H_2O, \quad (5)$$

$$Cu_2CO_3(OH)_2 + 2OH^- = 2CuO + CO_3^{2-} + 2H_2O. \quad (6)$$

Firstly, CO_3^{2-} hydrolyzes and generates OH^-. Then $Cu_4SO_4(OH)_6$ was synthesized by Cu^{2+}, SO_4^{2-} and OH^-. Because the solubility of $Cu_4SO_4(OH)_6$ is bigger than that of $Cu_2CO_3(OH)_2$, $Cu_4SO_4(OH)_6$ can be transferred into $Cu_2CO_3(OH)_2$, which is shown in Eq. (5). Finally $Cu_2CO_3(OH)_2$ reacts with the rest of OH^- to generate CuO. The overall reaction is shown in Eq. (7).

$$Cu^{2+} + 2CO_3^{2-} + H_2O \rightarrow CuO + 2HCO_3^-. \quad (7)$$

Because the hydrolyzation of CO_3^{2-} is a reversible reaction, CO_3^{2-} can not hydrolyze completely. And there is also no gas overflow in the process. The $CuSO_4 \cdot 5H_2O$: Na_2CO_3 molar ratio should be more than 2 (Eq. 7) in order to transform starting materials into CuO completely.

According to a series of single-factor experiments, the optimal condition of CuO synthesis is shown as follows: Na_2CO_3 and $CuSO_4 \cdot 5H_2O$ were mixed at the molar ratio of 3 : 1 and heated at 50°C for 5 h. The diameter of CuO nanoparticles which were calculated by Debye–Scherrer is approximately 6.4 nm at this optimal condition.

The morphology of as-prepared CuO nanostructures was analyzed by SEM, as shown in Figs. 4a, 4b. A pan-

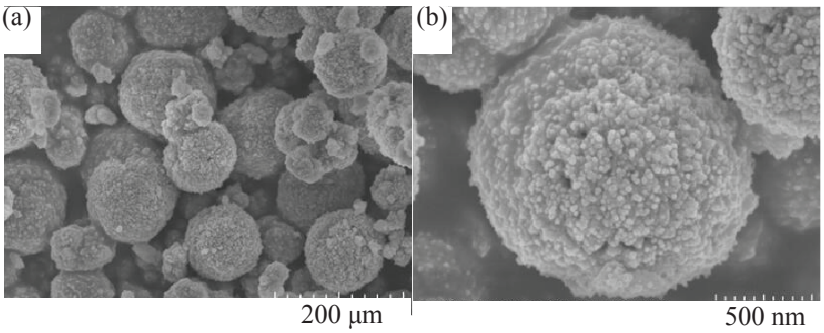

Fig. 4. SEM images of CuO sample prepared at optimal synthesis condition.

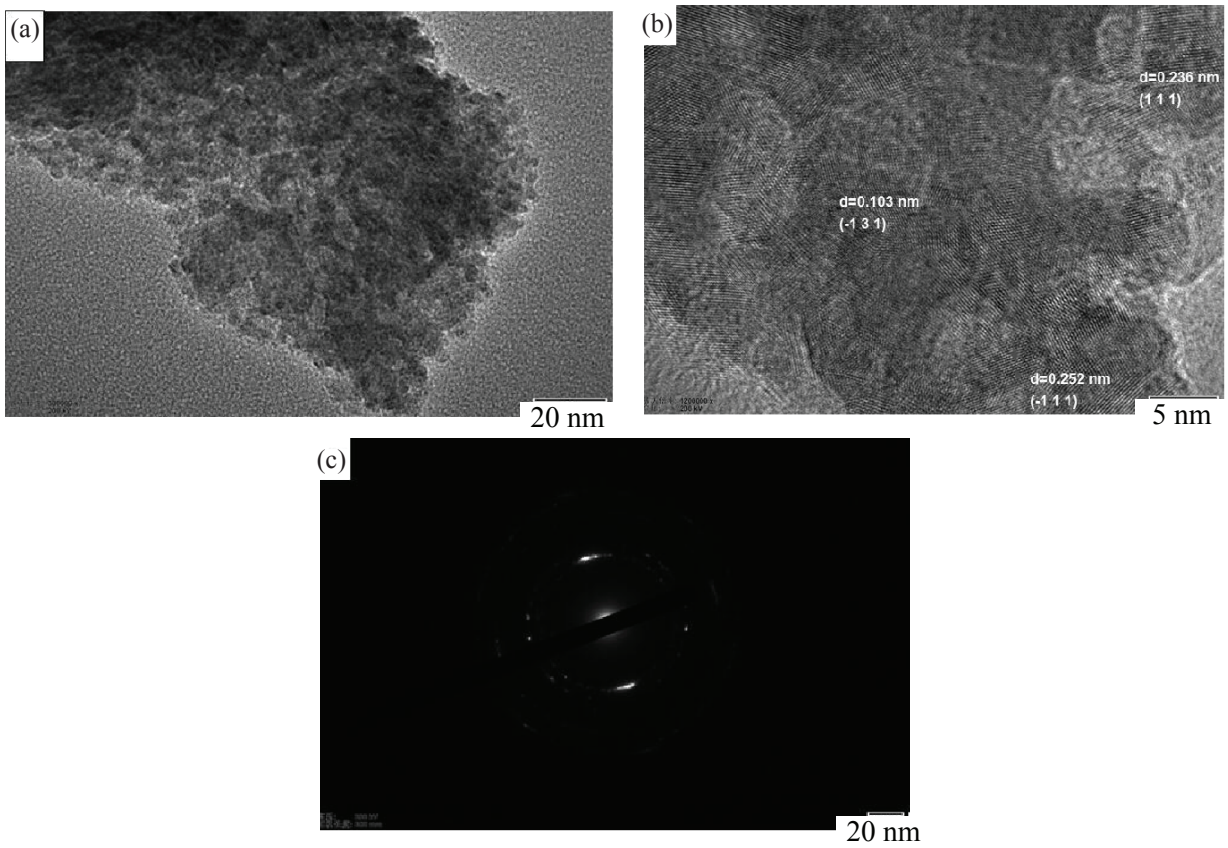

Fig. 5. (a) TEM, (b) HRTEM, and (c) SAED images of CuO sample prepared at optimal synthesis condition.

oramic morphology of CuO was shown in Fig. 4a, which was sphere-like with the diameter in the range of about 1.00–1.51 μm. A detailed morphology of CuO products was displayed in the high-magnification pattern (Fig. 4b), which showed that sphere-like CuO was composed of a large number of CuO nanoparticles.

Figure 5a is TEM image which shows the detailed structural characterization of the as-prepared CuO samples. TEM reveals that CuO samples were self-assembled by thousands of primary nanoparticles, which corresponds with the SEM images. The diameters of these nanoparticles are about 5.4 nm, which is consistent with the calculation of Debye–Scherrer in XRD. The crystal structure was examined by HRTEM in Fig. 5b. The fringe spacing is 0.236, 0.252, and 0.103 nm, which is consistent well with the distance of (111), (–111), and (–131) crystal face of CuO nanoparticles, respectively. From the homologous SAED image (Fig. 5c), the electron diffraction rings indicate the polycrystalline phase of CuO nanoparticles.

The application in AP decomposition. Figure 6 shows the DSC curves of pure AP and the mixture of AP with 2 wt % CuO nanoparticles at 10°C min^{-1}. For pure AP, the decomposition process could be divided into three steps. The first step is the crystallographic transition of AP from orthorhombic to cubic [29] at 248.5°C. The second step is low-temperature decomposition (LTD) which shows a peak at 338.7°C. LTD is a heterogeneous process, in which AP was partly decomposed into $HClO_4$ and NH_3 [30]. The process was shown as follows

$$NH_4ClO_4 \leftrightarrow NH_3{-}H{-}ClO_4 \leftrightarrow NH_3{-}HClO_4 \leftrightarrow NH_{3(a)} + HClO_{4(a)}. \quad (8)$$

High-temperature decomposition (HTD) is the third step of the decomposition of AP. In HTD process, AP dissociated and sublimated to $HClO_4$(g) and NH_3(g) simultaneously [30] at 453.9°C. The HTD process was shown in Eq. (9),

$$NH_{3(a)} + HClO_{4(a)} \leftrightarrow NH_3(g) + HClO_4(g), \quad (9)$$

The addition of CuO exerted little effect on the crystallographic transition and LTD of AP, but had a significant effect on HTD of AP.

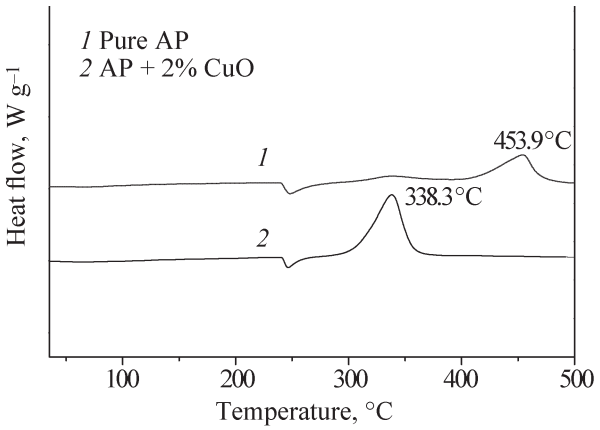

Fig. 6. DSC curve of thermal decomposition of pure AP and AP + 2 wt % CuO (10°C min^{-1}).

In Fig. 7, the temperature of endothermic phase transitions of AP with CuO nanoparticles at different heating rates (10, 15, 20, and 25°C min^{-1}) is almost identical to that of pure AP. The addition of catalyst played a little role on the crystallographic transition, but LTD and HTD were impacted by catalyst. Compared to the pure AP, the two exothermic peaks were coalesced into one. Meanwhile, the thermal decomposition temperature was decreased by 115.6, 110.5, 102.2 and 98.5°C (10, 15, 20, and 25°C min^{-1}, respectively). These results indicate that CuO nanoparticles show obvious catalytic activity in the thermal decomposition of AP.

Kinetic measurements. The kinetic parameters of AP decomposition were investigated through DSC data by Kissinger method [15, 30, 31]. Kissinger method was used to calculate the activation energy and the pre-exponential factor by the relation ship between the decomposition temperature and heating rate [15, 30], shown in Eq. (10),

$$\ln\left(\frac{\beta}{T_P^2}\right) = \ln\left(\frac{AR}{E_a}\right) - \frac{E_a}{RT_P} \qquad (10)$$

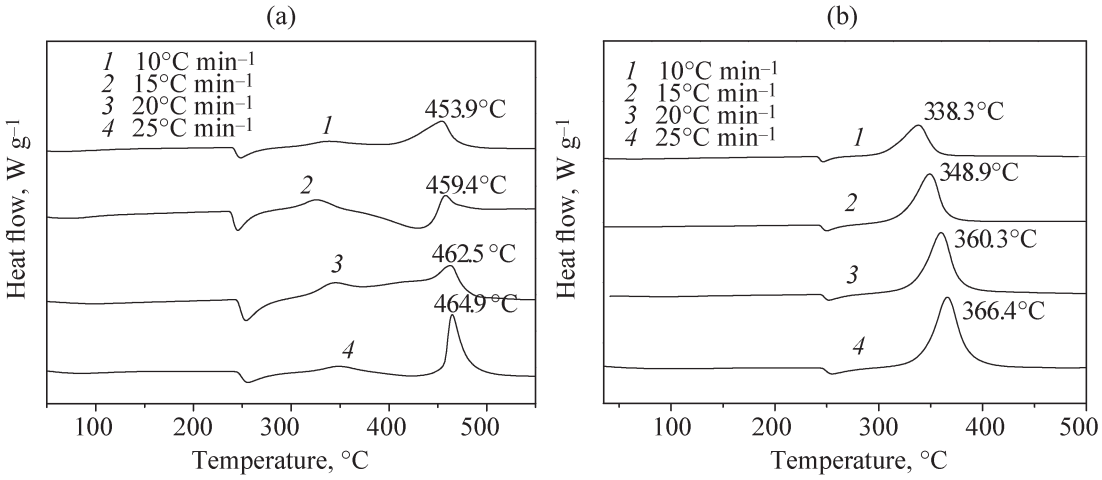

Fig. 7. DSC curves of (a) pure AP and (b) AP + 2 wt % CuO at given heating rates.

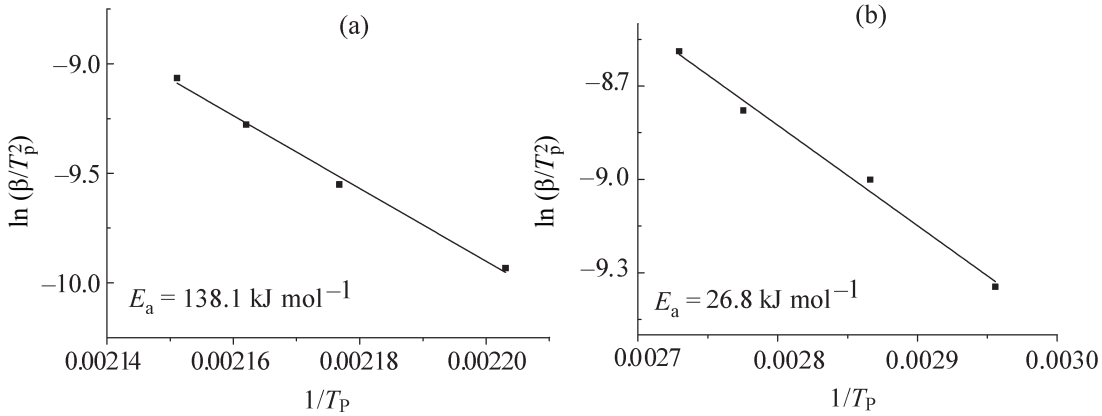

Fig. 8. Dependence of ln (β/T_p^2) on 1 TP for (a) pure AP and (b) AP + 2 wt % CuO decomposition.

where β is heating rate, T_P is the peak temperature, R is the gas constant, E_a is the activation energy, and A is the pre-exponential factor.

Figure 8 is straight lines plot of ln (β/T_p^2) against $1/T_P$ with pure AP and the mixture of AP with CuO nano-particles. The activation energy was calculated from the slope of the straight line. The slope of line is equal to $-E_a/R$.

For pure AP, the activation energy was 138.1 kJ mol^{-1}. The activation energy of AP decomposition in the presence of 2% CuO was reduced to 26.8 kJ mol^{-1}. The results indicate that the presence of CuO reduces the activation energy and the decomposition temperature of the decomposition of AP.

CONCLUSIONS

The CuO nanoparticles were synthesized by one-pot wet-chemical method using $CuSO_4 \cdot 5H_2O$ and Na_2CO_3 as starting materials. The reaction is mild, convenient and environmentally friendly. The diameter of CuO nanoparticles is about 6.4 nm. Moreover, the addition of CuO nanoparticles decreased activation energy of AP decomposition process and effectively promoted the thermal decomposition of AP.

REFERENCES

1. Tamuly, C., Saikia, I., Hazarika, M., and Das, M.R., *RSC Adv.*, 2014, vol. 4, pp. 53229–53236.
2. Bhattacharjee, A., and Ahmaruzzaman, M., *RSC Adv.*, 2016, vol. 6, pp. 41348–41363.
3. Seo, S.D., Jin, Y.H., Lee, S.H., Shim, H.W., and Kim, D.W., *Nanoscale Res. Lett.*, 2011, vol. 6, pp. 1–7.
4. Ramya, V., Neyvasgam, K., Chandramonhan, R., Valanarasu, S., and Benial, A.M.F., *J. Mater. Sci. Mater. Electron.*, 2015, vol. 26, pp. 8489–8496.
5. Zhu, Z., Zeng, W., Cao, S., and Chen, L., J. *Mater. Sci. Mater. Electron.*, 2015, vol. 26, pp. 9037–9043.
6. Gu, A., Wang, G., Zhang, X., and Fang, B., *Bull. Mater. Sci.,* 2010, vol. 33, pp. 17–20.
7. Huang, Q., Wang, Y., and Li, J., *Front. Chem. Eng. China*, 2007, vol. 1, pp. 256–260.
8. Habibi, M.H. and Karimi, B., *J. Therm. Anal. Calorim.*, 2014, vol. 115, pp. 419–423.
9. Zou, Y., Li, Y., Lian, X., and An, D., *Res. Mater. Sci.*, 2014, vol. 3, pp. 44–51.
10. Ayob, M.T.M., Ahmad, A.F., Mohd, H.M.K., Rahman, I.A., and Radiman, S., *AIP Conf. Proc.*, 2014, vol. 1614, pp. 8–13.
11. Jia, W., Reitz, E., Sun, H., Zhang, H., and Lei, Y., *Mater. Lett.*, 2009, vol. 63, pp. 519–522.
12. Wang, S.B., Wang, X.Q., Zhang, H.L., and Zhang, W.B., *J. Alloys. Compd.*, 2016, vol. 685, pp. 22–27.
13. Sadollahkhani, A., Ibupoto, Z.H., Elhag, S., Nur, O., and Willander, M., *Ceram. Int.*, 2014, vol. 40, pp. 11311–11317.
14. Sabbaghan, M., and Behbahani, B.M., *Mater. Lett.*, 2014, vol. 117, pp. 28–30.
15. Ayoman, E., and Hosseini, S.G., *J. Therm. Anal. Calorimeter.*, 2016, vol. 123, pp. 1213–1224.
16. Lu, L., and Huang, X., *Microchim. Acta*, 2011, vol. 175, pp. 151–157.
17. Singh, D.P., Ojha, A.K., and Srivastava, O.N., *J. Phys. Chem. C*, 2009, vol. 113, pp. 3409–3418.
18. Xu, X., Yang, H., and Liu, Y., *Cryst. Eng. Comm.*, 2012, vol. 14, pp. 5289–5298.
19. Ba, N., Zhu, L., Li, H., Zhang, G., Li, J., and Sun, J., *Solid State Sci.*, 2016, vol. 53, pp. 23–29.
20. Shaabani, B., Alizadeh-Gheshlaghi, E., Azizian-Kalandaragh, Y., and Khodayari, A., *Adv. Powder Technol.*, 2014, vol. 25, pp. 1043–1052.
21. Zhu, L., Chen, Y., Zheng, Y., Li, N., Zhao, J., and Sun, Y., *Mater. Lett.*, 2010, vol. 64, pp. 976–979.
22. Darezereshki, E., and Bakhtiari, F., *J. Min. Metall. Sect. B-Metall.*, 2011, vol. 47, pp. 73–78.
23. Zhang, Y., Ni, Y., and Ye, S., *RSC Adv.*, 2016, vol. 6, pp. 7086–7092.
24. Bakhtiari, F., and Darezereshki, E., *Mater. Lett.*, 2011, vol. 65, pp. 171–174.
25. Zhang, L., Yu, J.C., Xu, A.W., Li, Q., Kwong, K.W., and Yu, S.H., *J. Cryst. Growth*, 2004, vol. 266, p. 545–551.
26. Xue, B., Qu, C., Qian, Z., Han, C., and Luo, G., *Res. Chem. Intermed.*, 2016, pp. 1.
27. Parekh, H.S., and Hsu, A.C.T., *Ind. Eng. Chem. Prod. Res. Dev.*, 1968, vol. 7, pp. 222–226.
28. Alwan, A.K., and Williams, P.A., *Transition Met. Chem.*, 1979, vol. 4, pp. 319–322.
29. Cheng, Z., Chu, X., Xu, J., Zhong, H., and Zhang, L., *Ceram. Int.*, 2016, vol. 42, pp. 3876–3881.
30. Tian, S., Li, N., Zeng, D., Li, H., Tang, G., Pang, A., Xie, C., and Zhao, X., *Cryst. Eng. Comm.*, 2015, vol. 17, pp. 8689–8696.
31. Hosseini, S.G., Toloti, S.J.H., Babaei, K., and Ghavi, A., *J. Therm. Anal. Calorim.*, 2016, vol. 124, pp. 1243–1254.